National and Kapodistrian University of Athens
Department of Geology and Geoenvironment
Section of Geophysics and Geothermics

An upper crust shear-wave splitting study for the period 2013-2014 in the Western Gulf of Corinth (Greece)

Kaviris G., Kapetanidis V., Michas G. and Vallianatos F.

European Union
European Social Fund
Operational Programme
Human Resources Development, Education and Lifelong Learning
Co-financed by Greece and the European Union
ΕΣΠΑ 2014-2020
ανάπτυξη - εργασία - αλληλεγγύη

EGU General Assembly 2021

The Western Gulf of Corinth, Greece

The Corinth Rift, located in central Greece, is one of the most seismically active continental rifts in the world.

Since 2000, the Western Gulf of Corinth (WGoC) is continuously monitored by local stations of the Corinth Rift Laboratory (CRL) network (https://doi.org/10.15778/RESIF.CL), complemented by stations of the Hellenic Unified Seismological Network (HUSN; Evangelidis et al., 2021) and the Charles University of Prague.

The tectonics of the WGoC is constituted of roughly E-W normal faults, the largest of which being north-dipping, rooting at depth to a low angle dipping seismogenic zone (Bernard et al., 1997).

The most recent damaging earthquake has been the M_s=6.2 Aigion event that occurred on 15 June 1995, attributed to rupture on a low-angle, offshore blind fault (Bernard et al., 1997).

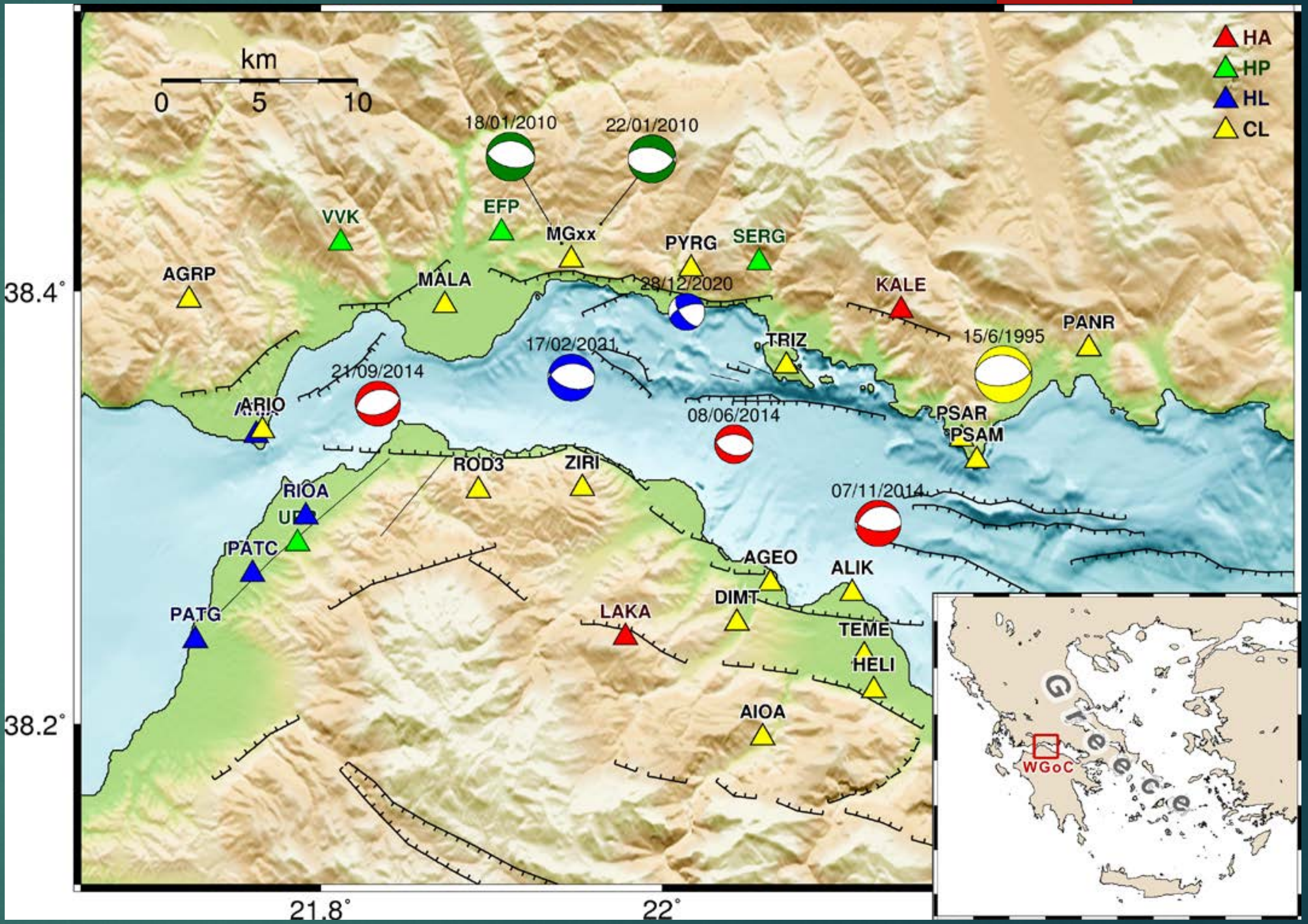

Focal mechanisms of significant earthquakes in the WGoC: yellow after Bernard et al. (1997), red after NKUA-SL, blue after GI-NOA, green after Sokos et al. (2012)

The Western Gulf of Corinth, Greece

In this study we focus on seismicity in the WGoC during 2013-2014, which can be summarized in the following significant episodes:

- May – November 2013: seismic swarm near Helike (group #9, blue), divided in three stages starting on 21 May, 14 July and 26 October 2013, respectively, including several events with 3.5 ≤ M_w ≤ 3.7 (Kapetanidis et al., 2015; Kaviris et al., 2017)
- October 2013 – September 2014: Swarm in the offshore region of Nafpaktos-Psathopyrgos (group #4, green), culminating with an M_w=4.9 event on 21 September 2014.
- June 2014: aftershock sequence (group #8, brown) following an M_w=4.5 event on 8 June 2014.
- November 2014: aftershock sequence (group #6, red) following an M_w=5.0 event on 7 November 2014 (Kaviris et al., 2018).

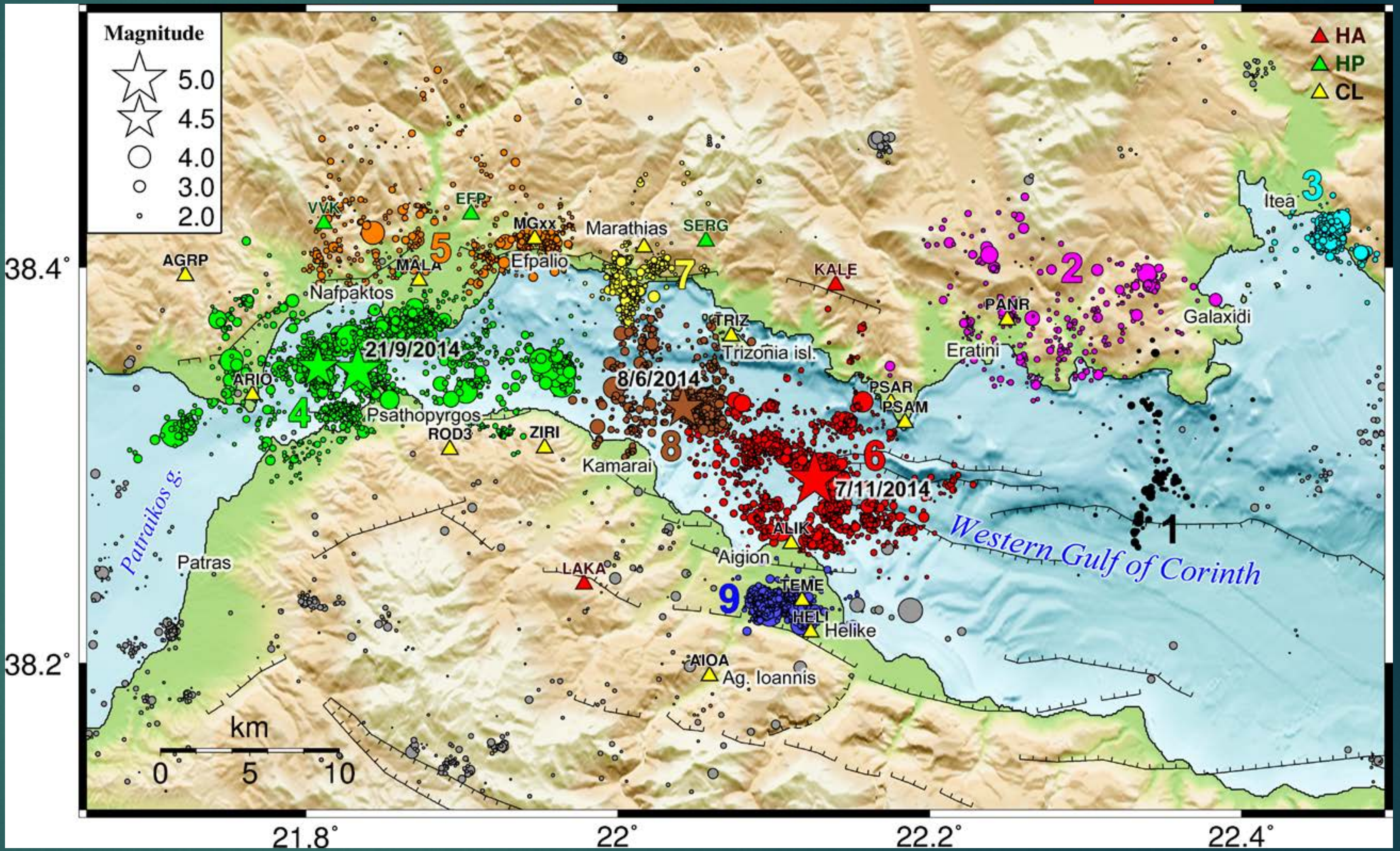

Determination of hypocenters

A dataset of over 9000 manually analyzed events was employed.

Seismicity was divided into 9 groups, according to their spatial clustering, which were further processed individually. Hypocenters of the broader region or deeper than 15 km were placed in a 10th "miscellaneous" group (gray).

Initial location was performed with the HypoInverse code (Klein, 2002), using the Rigo et al. (1996) velocity model for the WGoC, except for the Helike 2013 swarm, for which a custom model for that sequence was used (Kapetanidis et al., 2015)

Catalogue and cross-correlation differential travel-time data were employed to perform double-difference relocation with the HypoDD algorithm (Waldhauser, 2001), separately for each group .

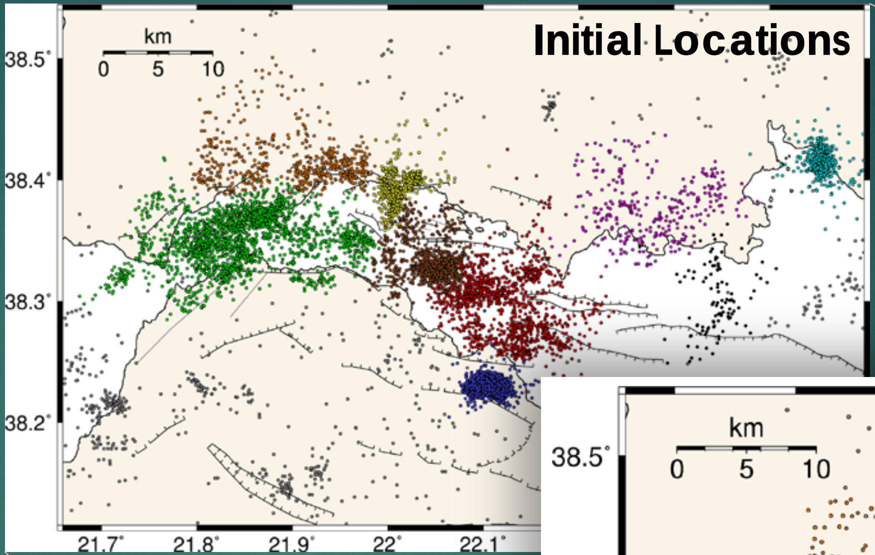

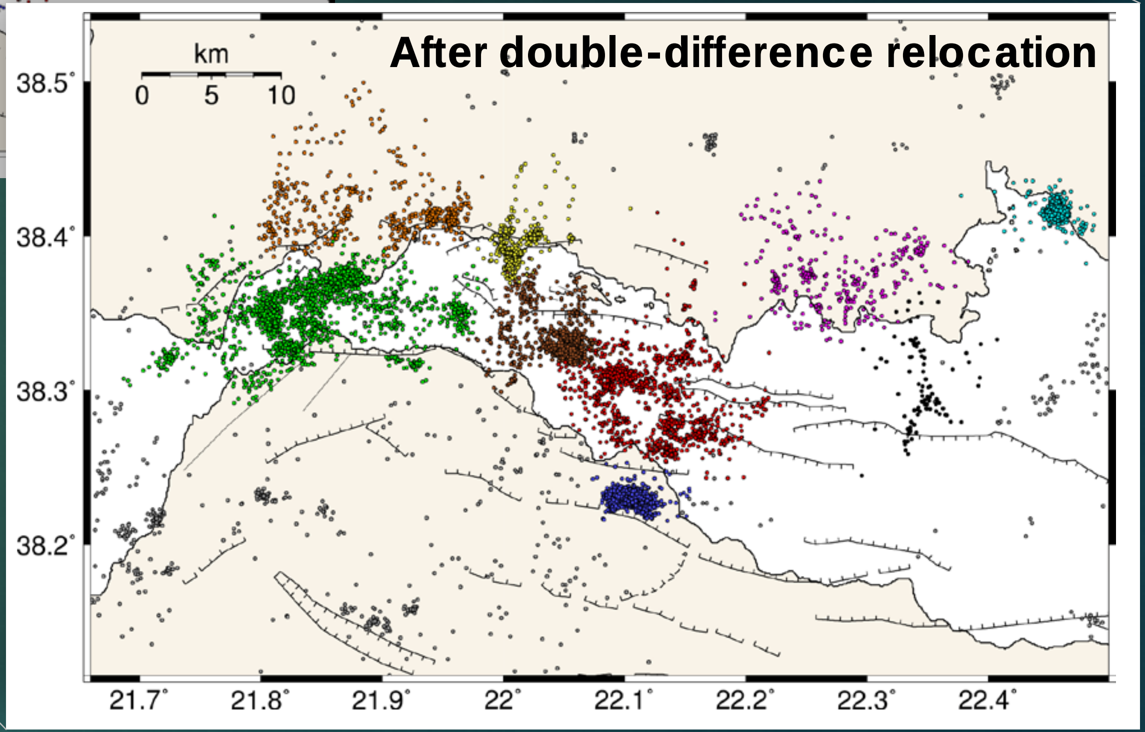

Determination of hypocenters

A total of 8944 events were successfully relocated.

Seismicity is mainly concentrated on a low angle seismogenic weak layer at depths between 6.5 and 10 km below the gulf.

Several clusters indicate activation of higher-angle faults, rooting at the low-angle seismogenic layer.

Northernmost seismicity (groups #2 and #5) indicates sparse activity on a shallow-angle north-dipping plane with a roughly constant background rate, associated with a proposed growing immature detachment (Lambotte et al., 2014)

The westernmost part of the Nafpaktos-Psathopyrgos group #4 (green), mostly activated after the 21 September 2014 M_w=4.9 event, is possibly associated with the Rion-Patras SW-NE-trending dextral oblique-normal fault zone.

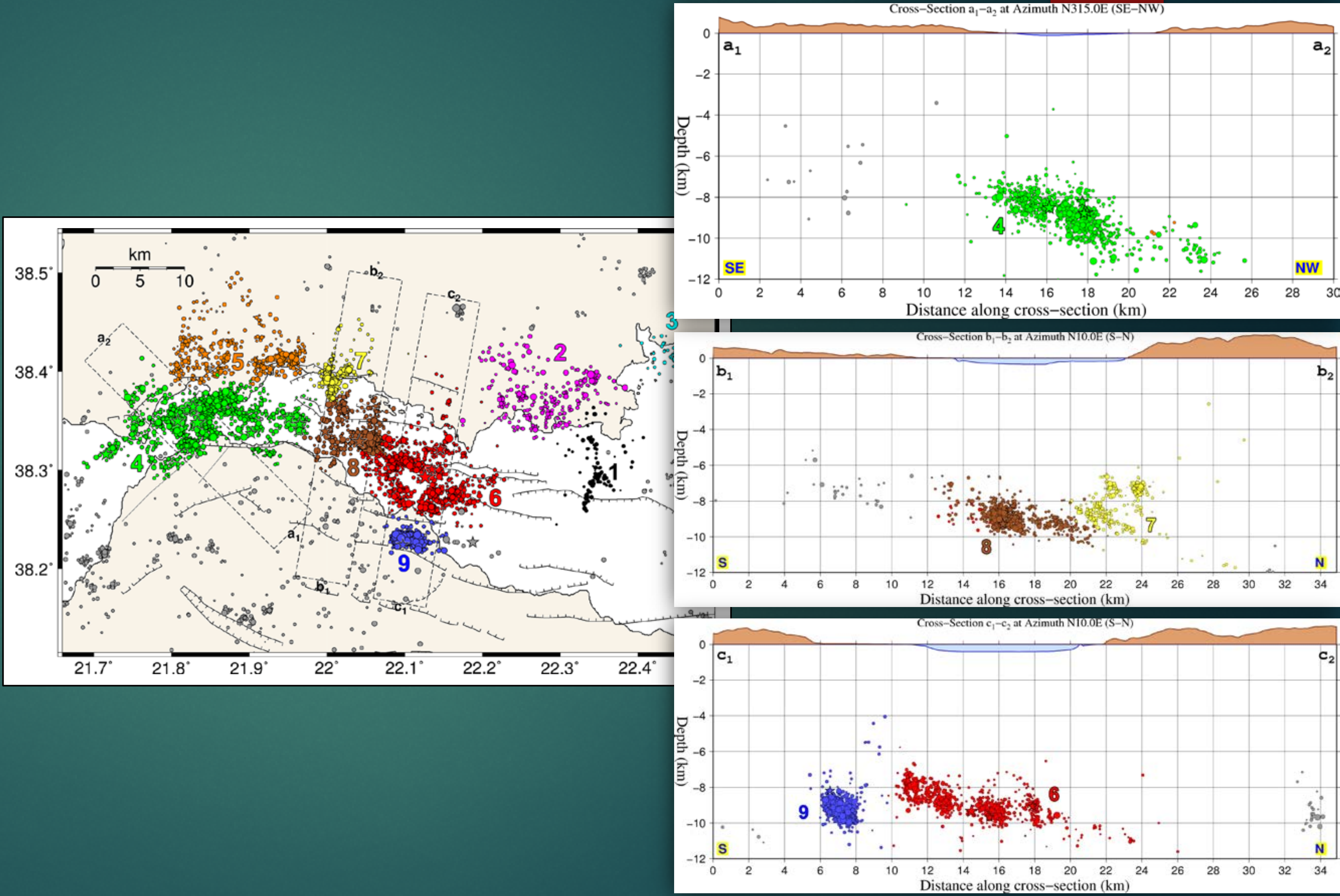

Shear-wave Splitting

Inhomogeneities in the upper crust may cause anisotropic effects to the velocity of seismic shear-waves as they propagate through the medium.

As an effect, shear-waves can be split in two components: one that becomes polarized to a vertical plane, oriented at a direction φ, which promotes a faster propagation velocity (S_{fast}) and a slower perpendicular component S_{slow}.

The two split shear-waves arrive at a station with a time-delay t_d, which depends on the degree of anisotropy and the length of the seismic ray that has propagated through the anisotropic medium.

Seismic anisotropy of the upper crust is attributed either to the existence of fluid-filled microcracks, whose geometrical characteristics and alignment depend on the applied stress field, or to the orientation of faults in the vicinity of the receiver.

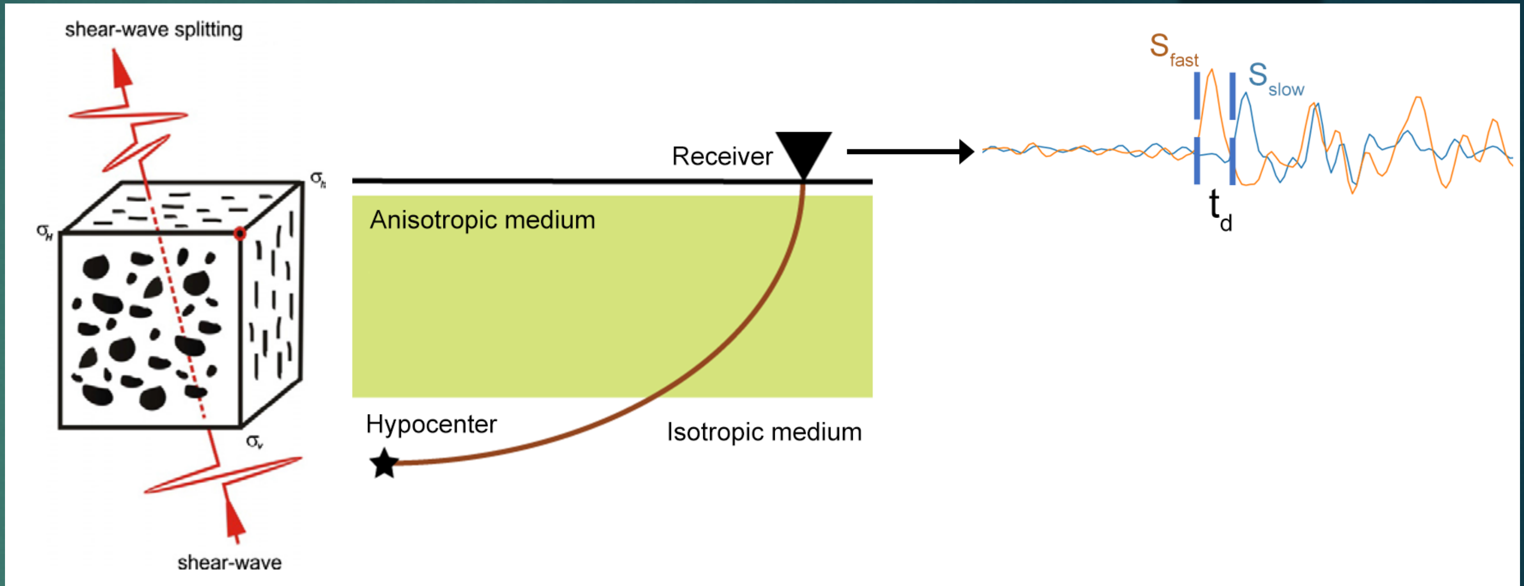

The study of shear-wave splitting parameters can provide information on the direction of the maximum horizontal stress component, S_{Hmax}, in the region, which affects the anisotropic properties of the medium through which the received seismic rays have propagated.

Shear-wave Splitting Measurements

To measure the shear-wave splitting (SWS) parameters at a station, events within the “shear-wave window” are selected, i.e. events whose seismic rays have an angle of incidence at the surface of less than 45°, to avoid the influence of converted pS phases which may be superimposed with the direct S-waves arrival.

Signal-to-noise ratio (SNR>1.5) criteria are also imposed to ensure that the processed S-waves are adequately clear.

In the present study, we apply an automated shear-wave splitting analysis with the open-source Pytheas software (Spingos et al., 2020).

Band-pass filter is applied to the velocity recordings prior to processing, to remove long-period and high-frequency noise, enhancing the SNR.

A quality grade (A to E) is assigned to each SWS measurement, according to the resulting errors of φ and t_d, and, optionally, to the correlation coefficient between the two horizontal components after the removal of the anisotropic effect. This permits the rejection of potentially erroneous measurements.

In addition, SWS measurements whose φ direction is either nearly perpendicular or parallel to the polarization direction p of the corrected shear-wave are discarded (“null” events), as in those cases neither the S_{fast} polarization direction nor the time-delay t_d can be safely determined (Wüstefeld and Bokelmann, 2007).

https://github.com/ispingos/pytheas-splitting

Shear-wave Splitting Measurements

2013 – 01 – 01T11 : 13 : 13.800; CL. PSAR EV
baz: 260.0N°E, **ain**: 7.7°, **epi**: 2.1 km **mag :** 2.0
φ : 103.0 ± 4.6 N°E, $\mathbf{t_d}$: 70.00 ± 0.65 ms , **p :** 153.9N°E, **grade :** A, **flt :** 0.5 | 5.0 Hz

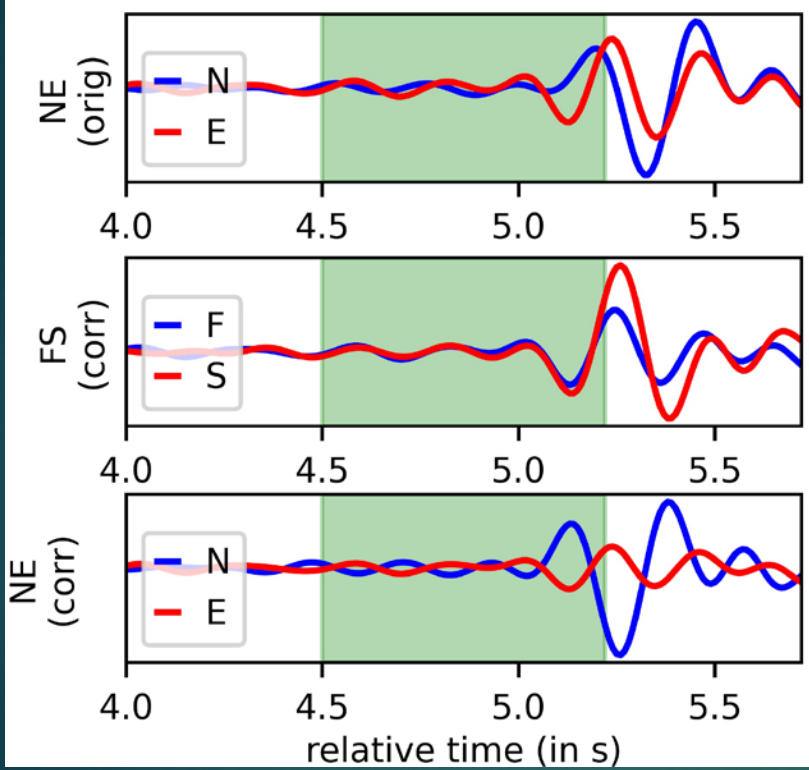

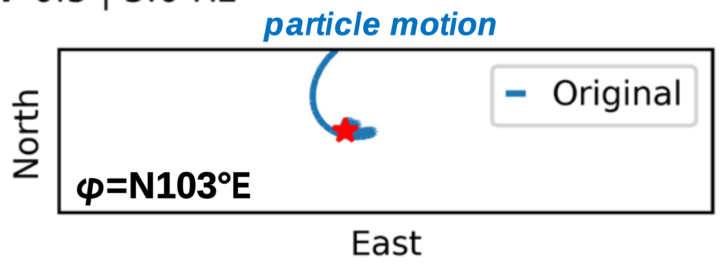

Step #1: Measuring of the S_{fast} polarization direction (φ=N103°E)

Step #2: Rotating to the S_{fast}/S_{slow} (FS) co-ordinate system, measuring the time-delay (t_d=70ms) and shifting S_{slow} by t_d

Step #3: Rotating waves back to the N-S/E-W co-ordinate system and measuring the source polarization direction (p=N154°E) after the anisotropy correction

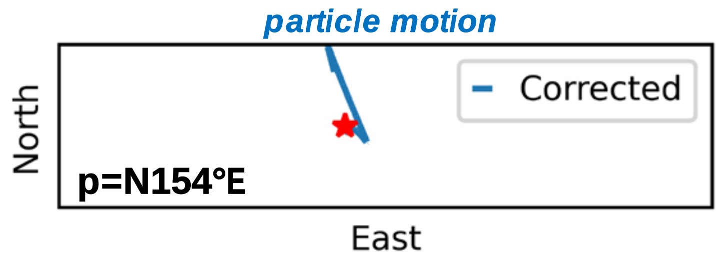

In the presented example, a Shear-wave Splitting measurement was performed with the Pytheas software (Spingos et al., 2020), following the abovementioned 3 steps.

Shear-wave Splitting Measurements

The S_{fast} polarization direction, φ, is determined along with the time-delay between S_{fast} and S_{slow}, t_d, by means of the Eigenvalue (EV) method (Silver and Chan, 1991).

Supposing linear polarization of the S-waves at the receiver, the eigenvector corresponding to the major eigenvalue λ_1 should describe the fast S-wave signal, whereas the other eigenvector represents noise and λ_2 the respective noise magnitude.

The best combination of φ and t_d is decided by the global minimum of the minor eigenvalue λ_2 (contours diagram on the right).

Calculations are performed in a selected waveform window highlighted in green.

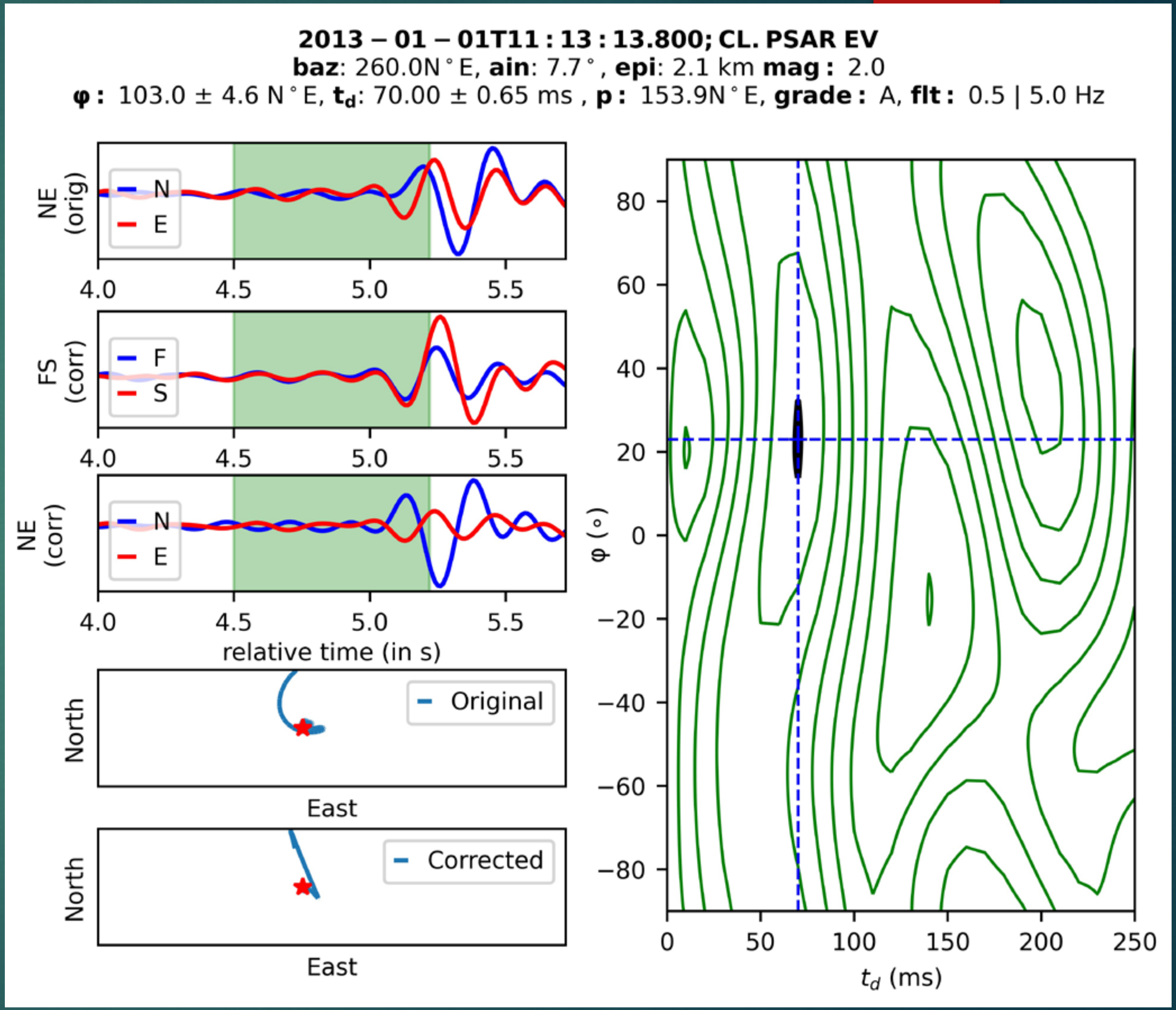

Shear-wave Splitting Measurements

The optimal S-wave window is determined using Cluster Analysis (Teanby et al., 2004), as implemented by the Pytheas software (Spingos et al., 2020).

A series of different window lengths, based on the picked S-wave arrival-time, are tried out. The φ and t_d solution pairs for different windows are examined and the most constrained cluster with the smaller errors is selected.

Following the automatic filtering algorithm of Savage et al. (2010), a range of predefined band-pass Butterworth filters are tested in each case and the one that yields the highest SNR is selected.

A subset of the automatic measurements was verified by manual SWS analysis in order to calibrate the parameters of the procedure.

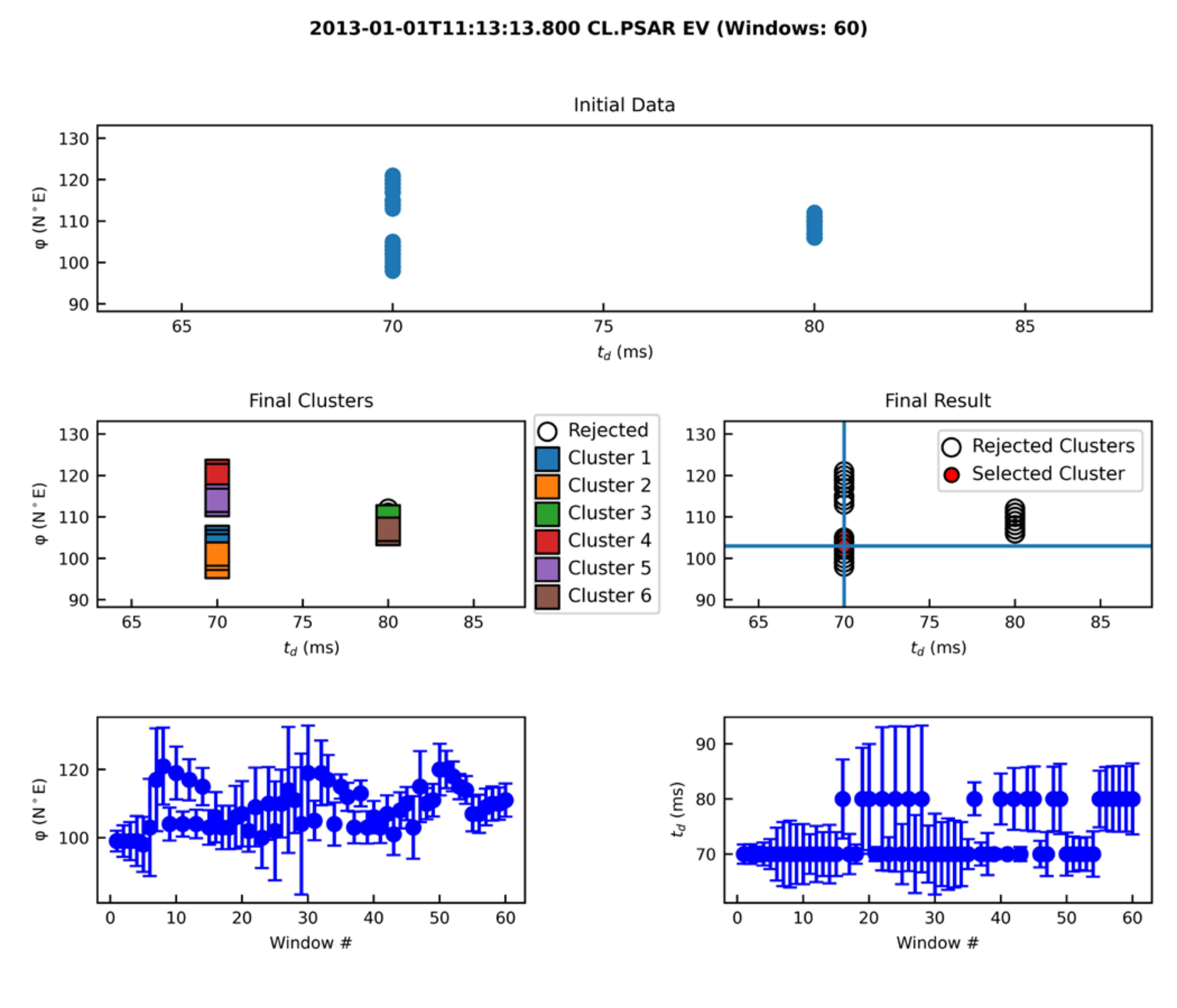

Shear-wave Splitting Results

The S_{fast} polarization direction (φ) measurements at each station are presented in the form of rose diagrams.

In most cases there is a strong preference for a main φ orientation in a general E-W direction.

A small number of measurements can be detected where φ is significantly different from its dominant value.

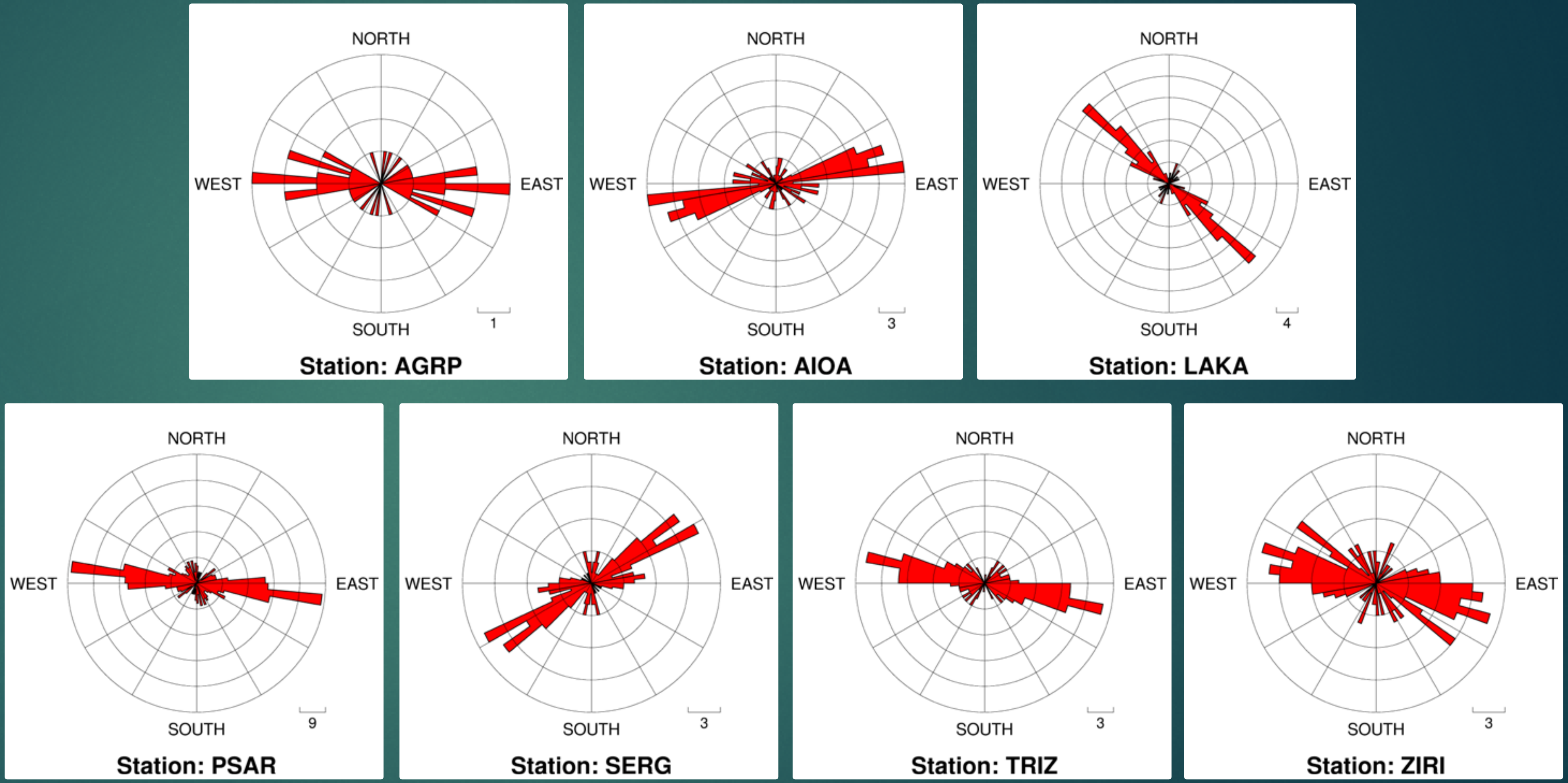

Shear-wave Splitting Results

The φ, t_d measurements, along with the respective azimuth and angle of incidence, are presented in the form of equal-area projections for each station (triangle at the center). The bar length is proportional to t_d and oriented according to φ.

In some cases, a spatial dependence for a subset of the measured φ values can be observed, although the majority of orientations are consistent with the dominant φ.

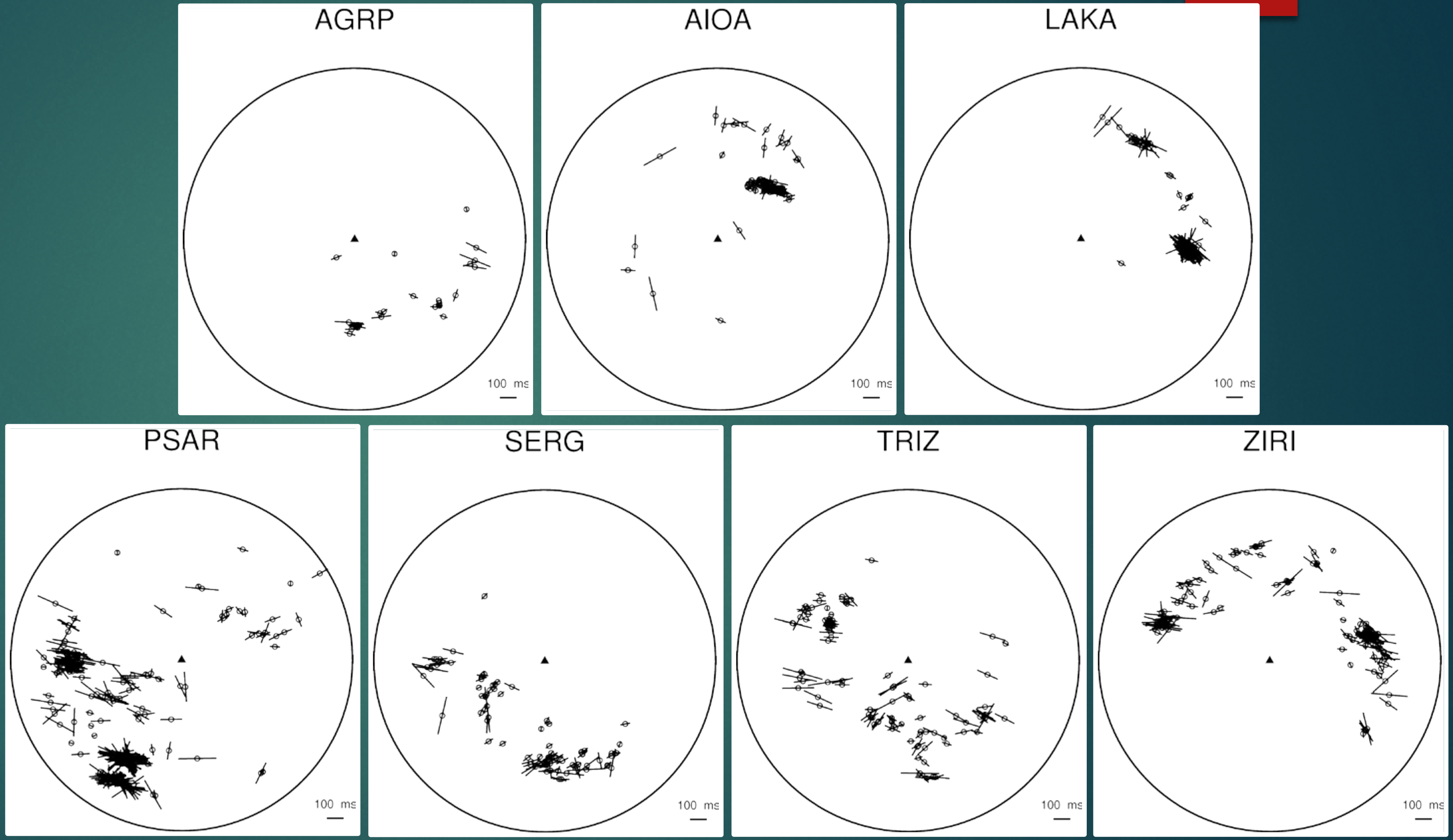

Shear-wave Splitting Results

- In total, 746 events provided 832 valid measurements with A, B or C quality grade in the 7 selected stations.
- 2244 candidate events were also examined, providing 5368 measurements which, however, were rejected, as they either yielded a low quality grade (D or E) or were found to be *null* (φ direction sub-parallel or sub-perpendicular to the direction *p* of the corrected shear-wave).
- Mean S_{fast}-S_{slow} time-delays t_d range 62-135 ms.
- Normalized time-delays t_n range 5.1-9.3 ms/km.

Station	N	$\bar{\varphi}$ (°)	$\delta\bar{\varphi}$ (°)	t_d (ms)	δt_d (ms)	t_n (ms/km)	Δt_n (ms/km)
AGRP	27	88.7	11.7	72.2	9.1	5	0.6
AIOA	104	79.4	7.7	62.4	3.7	5.2	0.3
LAKA	102	134.7	5.9	117.5	5.1	8.1	0.3
PSAR	287	99.9	4.8	134.5	3.8	9.3	0.3
SERG	87	58.4	7.5	86	6.1	6.6	0.5
TRIZ	101	96.7	5.8	101.1	5.5	8.5	0.5
ZIRI	124	106.2	7.3	106.5	5.2	8.1	0.4

Temporal Variations of Time-delays

Changes in the temporal characteristics of the shear-wave splitting parameters can be related to subtle alterations in the local stress-field or to the diffusion of fluids through the microcrack network, according to the Anisotropic Poro-Elasticity (APE) model (Crampin & Zatsepin, 1997).

The S_{fast}-S_{slow} time-delays, t_d, depend on the length of the seismic ray that propagates through the anisotropic medium. To take this effect into account, normalized time-delays $t_n=t_d/R$ are calculated, where R is the hypocentral distance.

Patterns of temporal variations in t_n have been attributed to the preparatory stage of significant earthquakes, e.g. before the 1986 Ms=6.0 earthquake in North Palm Springs, southern California (Crampin et al., 1990), before an M=5 event in 1998 in SW Iceland (Figure on the left; Crampin et al., 1999) or before an M=4.9 event in northern Iceland in 2002 (Gao and Crampin, 2006). A gradual increase in t_n has been associated with the accumulation of tectonic stress in the area prior to the occurrence of an earthquake.

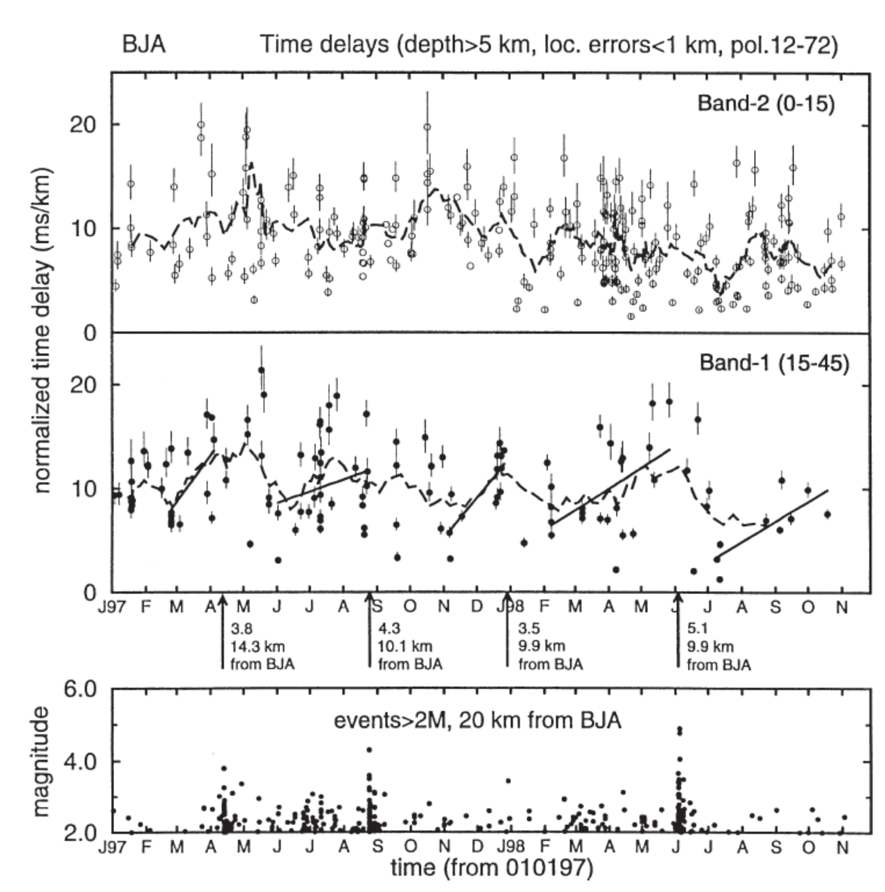

Example of stress-forecast using t_n variations from Crampin et al. (1999)

Temporal Variations of Time-delays - Results

A histogram with the number of events per day is displayed on top, where the initiation of significant seismic episodes is marked, along with the respective cluster number (C#).

The bottom panels show the temporal variation of normalized time-delays, t_n, at stations SERG and TRIZ. Colored circles indicate quality grade (A-C). The bold red line is the smoothed moving average in 3-point windows and the dashed red line the respective standard error of the mean. Stars at the bottom indicate the occurrence of significant earthquakes with $M_w \geq 5.0$ (red), $4.5 \leq M_w < 5.0$ (green) or $4.0 \leq M_w < 4.5$ (blue).

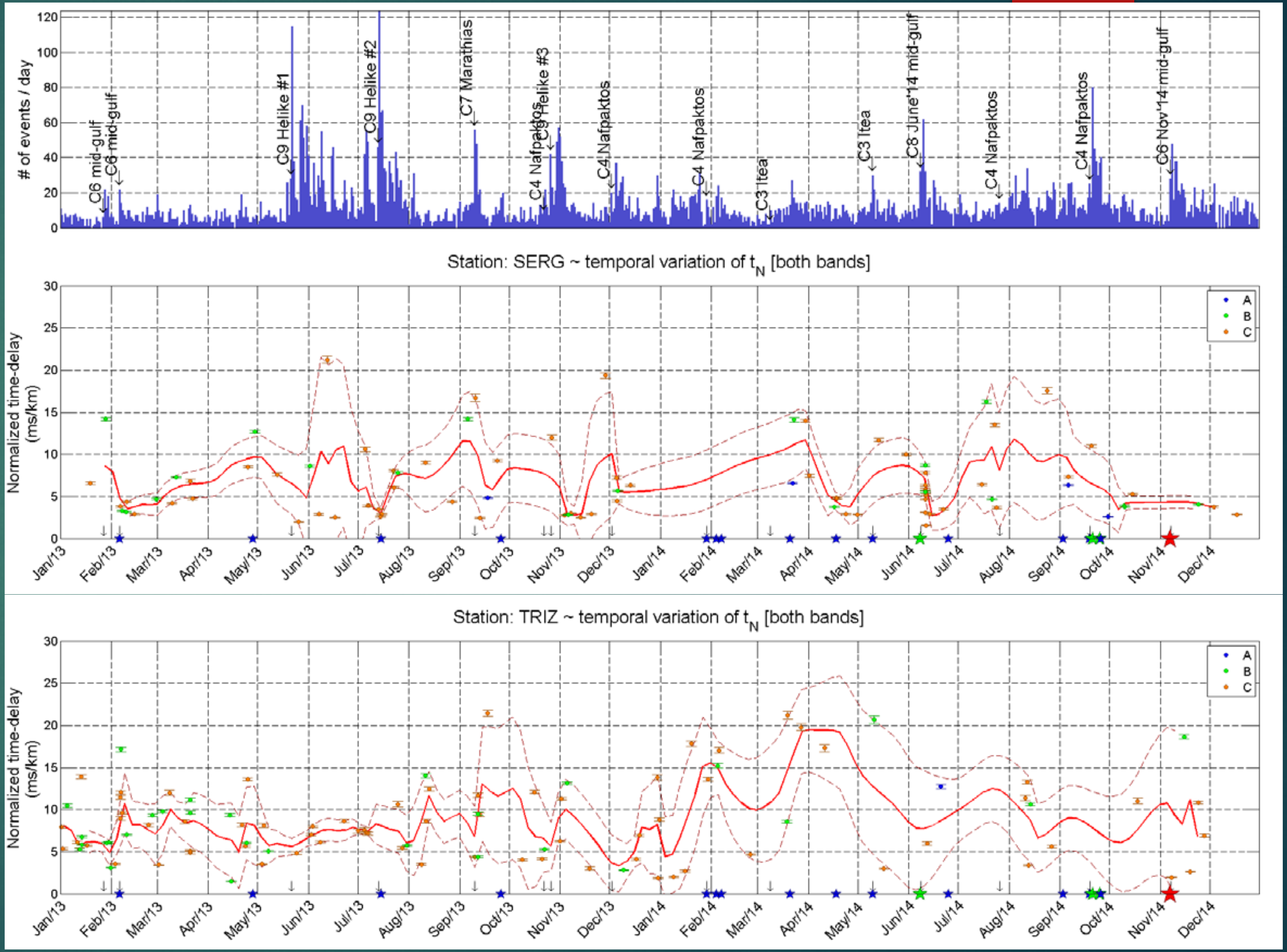

Temporal Variations of Time-delays - Results

The measurements are refined by selecting those whose ray-paths belong to "Band-1". This is defined as the double-leafed solid angle between 15° and 45° on either side of the micro-crack plane (Crampin et al., 1999), whereas those within ±15° from the crack plane belong to "Band-2".

Time-delays grouped in "Band-1" are considered to be sensitive to changes in the aspect-ratio of microcracks, whereas "Band-2" measurements are more dependent on the density of microcracks (Crampin et al., 1999).

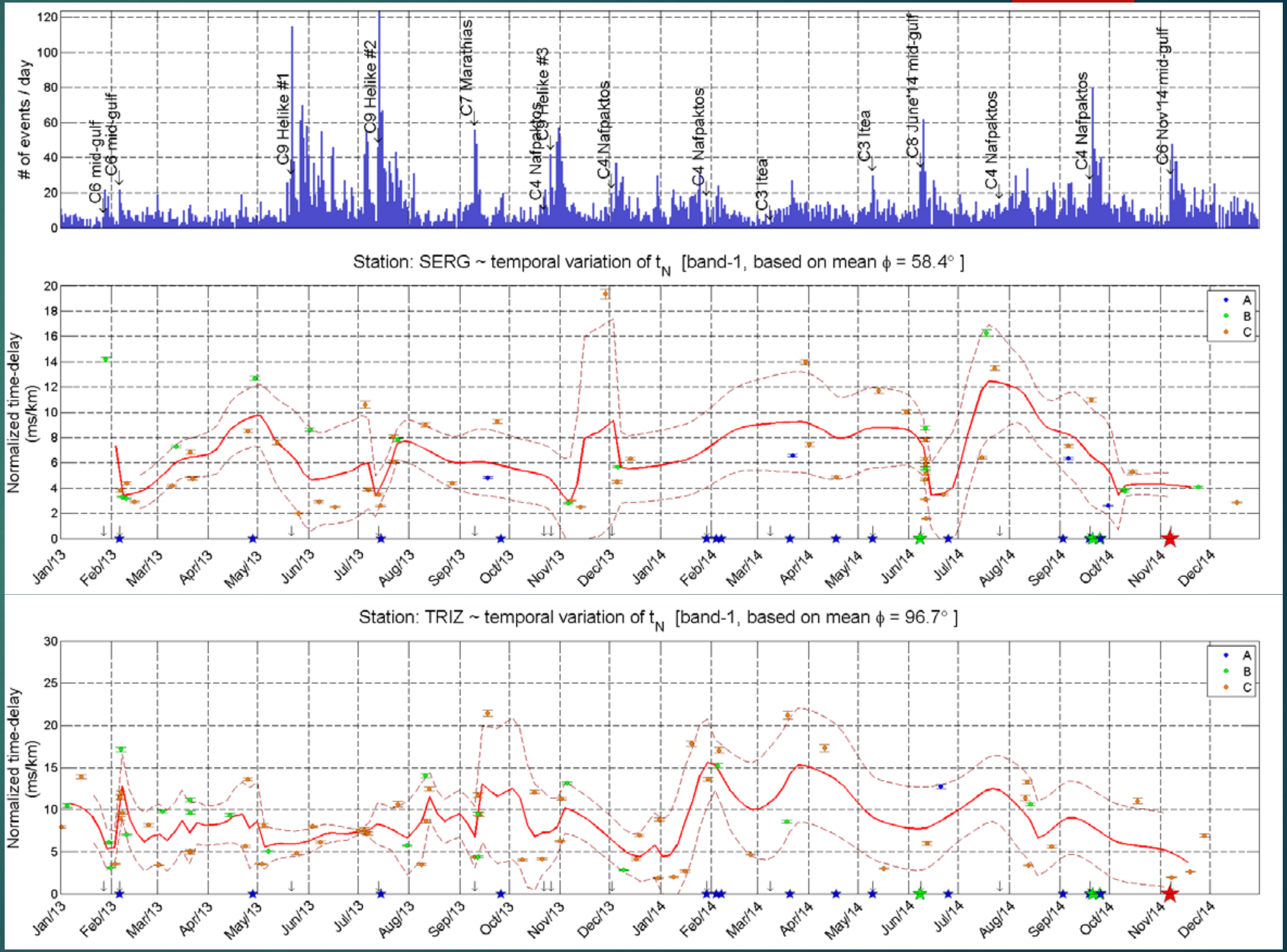

Temporal Variations of Time-delays - Results

To detect possible linear correlations in the temporal changes of time-delays, we apply a series of linear regressions in sliding windows of variable lengths.

In the bottom panels, bold solid lines correspond to linear regressions for which the Student's t-test for statistical significance yields a $p<0.05$ for the probability of zero slope, whereas dotted lines are for $p>0.05$. The color corresponds to the linear correlation coefficient.

There are some indications for gradual increase of t_n at SERG before the beginning of the Helike swarm (February-May 2013). Reducing t_n values are observed at both SERG and TRIZ during a swarm initiated between Nafpaktos-Psathopyrgos in July-October 2014 and before the M_w=5.0 event on 7 November 2014.

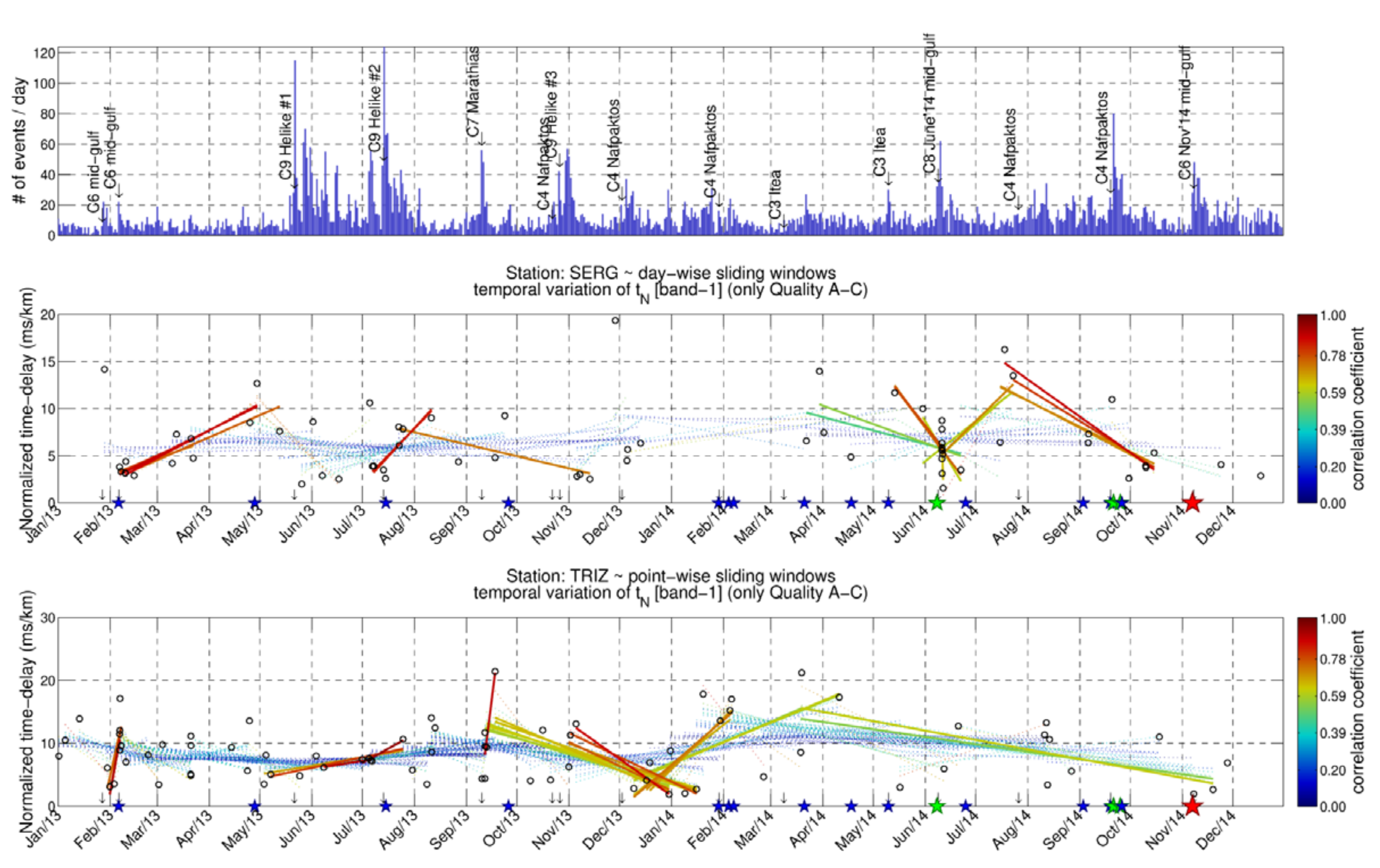

Temporal Variations of Time-delays - Results

Station ZIRI exhibits decrease of t_n in February-April 2013, before the beginning of the 2013 Helike swarm, followed by generally weak correlations.

A further refinement is performed by retaining measurements whose φ is within the $\bar{\varphi} \pm 30°$ range of the respective station (bottom panel).

This enhances the image for station ZIRI, where a weak increase of t_n can be observed in the first half of 2014, especially after the 8 June 2014 event, followed by a decrease during the July-October Nafpaktos-Psathopyrgos swarm, before the M_w=5.0 event of 7 November 2014.

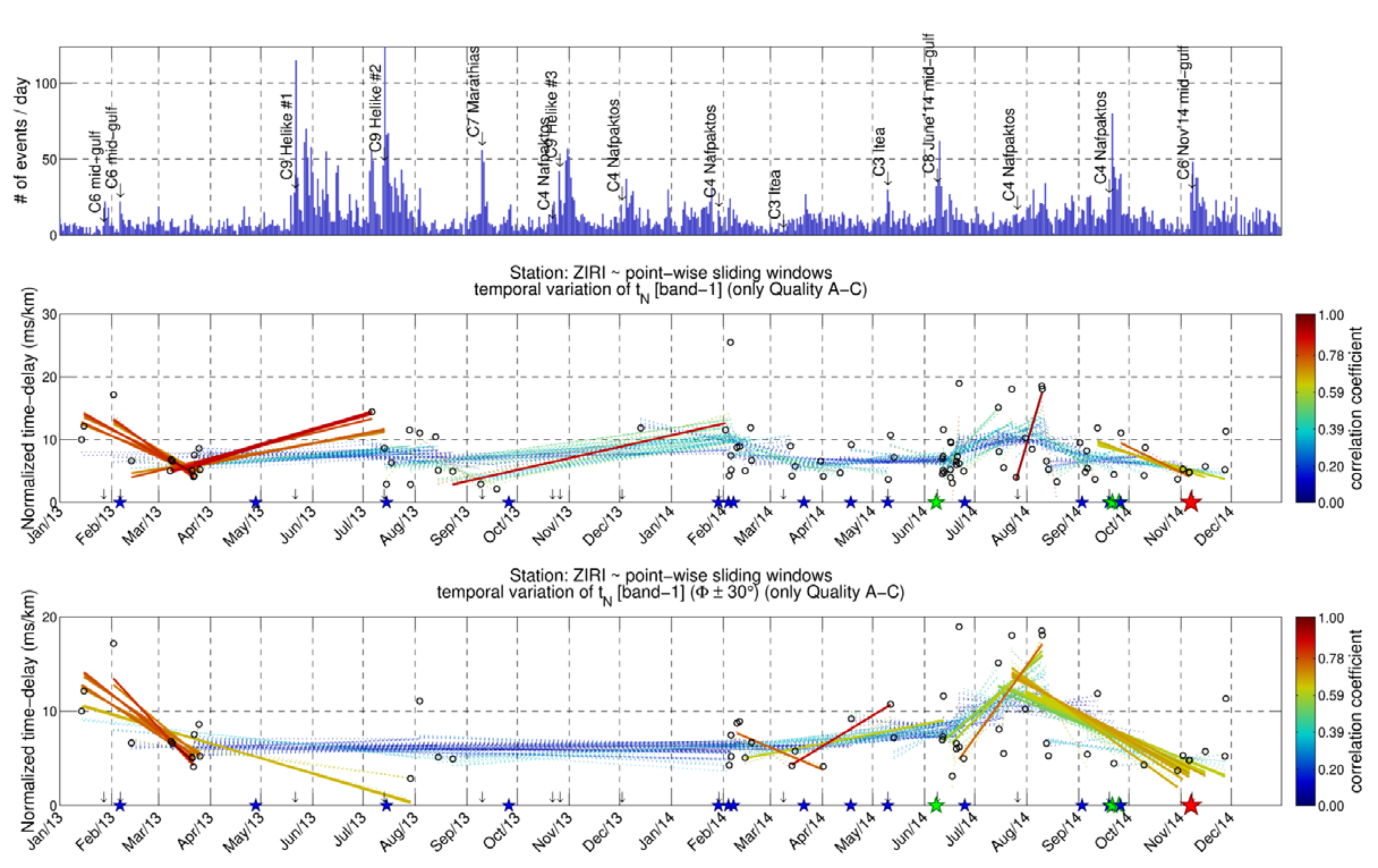

Comparison with previous studies

The results of the present study, derived by a fully automatic processing method, are compared with manual SWS measurements of previous studies in the WGoC (Kaviris et al., 2017, 2018).

Average φ directions are consistent, as shown in the rose diagrams on the right. This suggests that the automatic method manages to extract the dominant φ direction successfully.

Furthermore, as the automatic method is free of potential analyst biases, it also confirms the integrity of the manually derived measurements by visual inspection of polarigrams and hodograms (Kaviris et al., 2017, 2018).

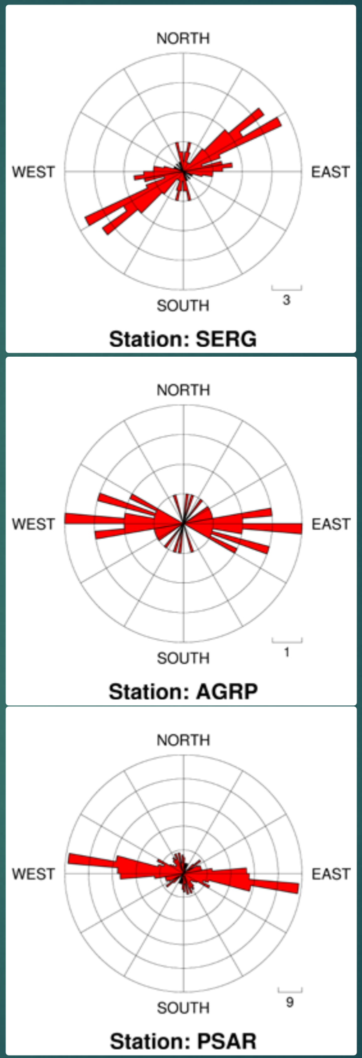

(This study)

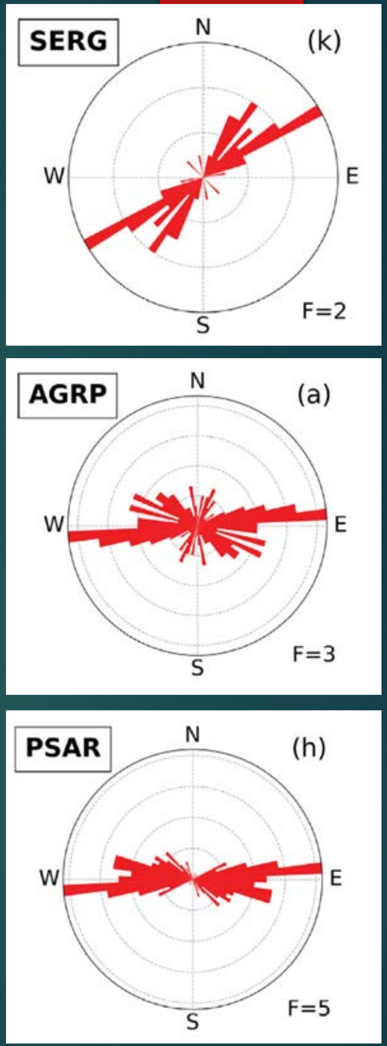

(Kaviris et al., 2018)

Comparison with previous studies

Likewise, comparable temporal variations of t_n were observed for stations ZIRI and SERG by Kaviris et al. (2018), where a weak decrease pattern was observed before the 7 November 2014 event.

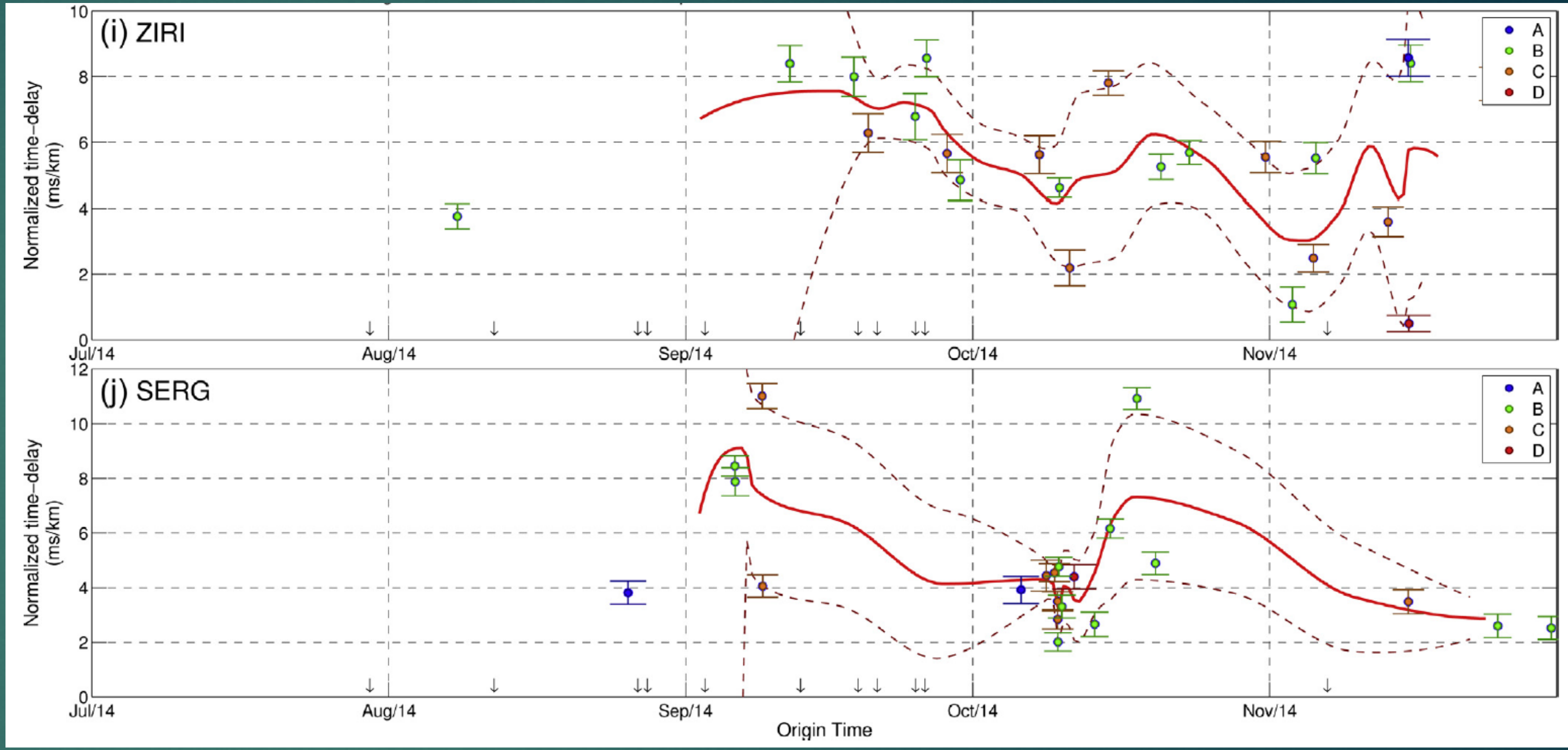

Figure from Kaviris et al. (2018)

Conclusions

- The mean polarization directions are consistent with either the horizontal compressive stress (S_{Hmax}) which in the WGoC is in a roughly E-W direction (e.g. Kapetanidis & Kassaras, 2019) or with the orientation of local faults.
- A secondary φ direction is mainly observed in southern stations, which tend to be oriented WNW-ESE (e.g. LAKA, ZIRI).
- The S_{fast} polarization direction at station SERG is NE-SW, consistent with previous results from manual SWS measurements (e.g. Kaviris et al. 2017, 2018), possibly related to local structures.

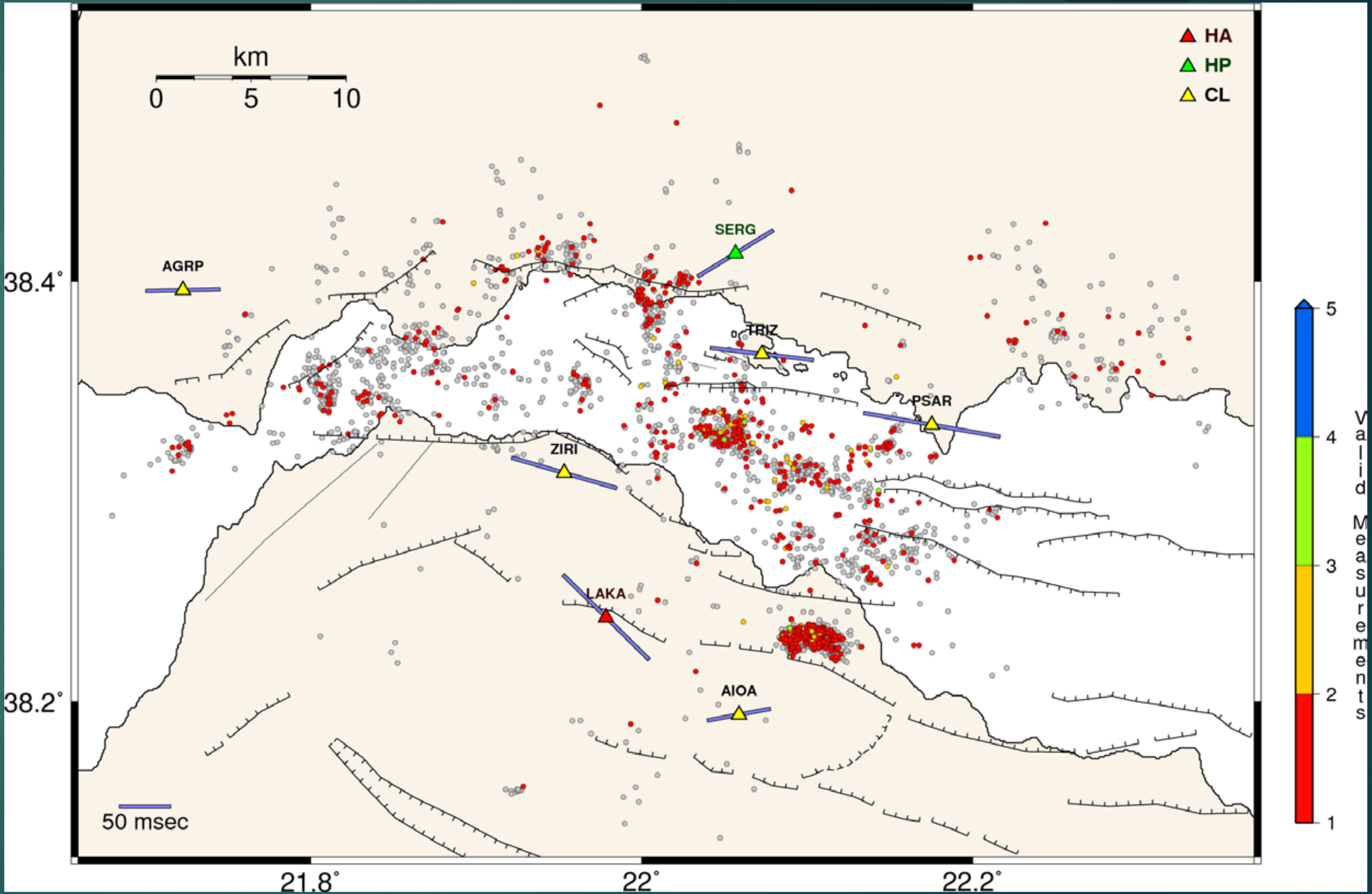

Conclusions

- Temporal variations of normalized time-delays t_n can be detected, albeit with significant degree of scattering.
- Possible relation of temporal changes of t_n with subtle variations of the stress-field or due to the diffusion of fluids may be considered only after the application of more strict selection criteria.
- These criteria include exclusion of Band-2 measurements, considered to be less sensitive to stress-changes, exclusion of measurements with φ values significantly different from the dominant direction, and selections by clusters to exclude possible spatial dependence in the observed variations.

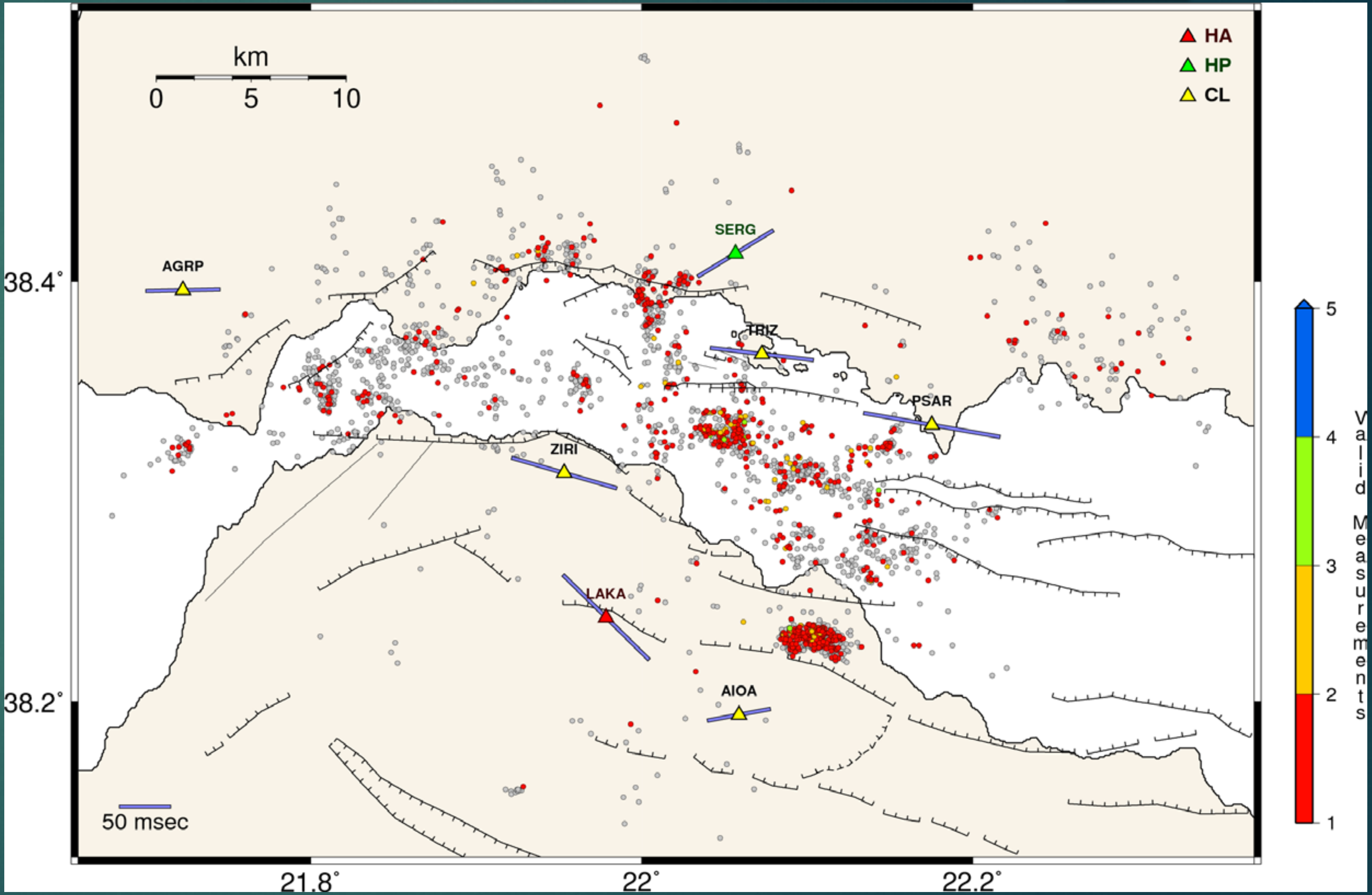

Acknowledgments

We would like to thank the personnel of the Hellenic Unified Seismological Network (http://eida.gein.noa.gr/) and the Corinth Rift Laboratory Network (https://doi.org/10.15778/RESIF.CL) for the installation and operation of the stations used in the current article.

The present research is co-financed by Greece and the European Union (European Social Fund- ESF) through the Operational Programme «Human Resources Development, Education and Lifelong Learning 2014-2020» in the context of the project "The role of fluids in the seismicity of the Western Gulf of Corinth (Greece)" (MIS 5048127).

European Union
European Social Fund

Operational Programme
Human Resources Development,
Education and Lifelong Learning

Co-financed by Greece and the European Union

ΕΣΠΑ
2014-2020
ανάπτυξη - εργασία - αλληλεγγύη

References

Bernard, P., Briole, P., Meyer, B., Gomez, J., Tiberi, C., Berge, C., Cattin, R., Hatzfeld, D., Lachet, C., Lebrun, B., Deschamps, aA., Courboulex, F., Larroque, C., Rigo, Aa., Massonnet, D., Papadimitriou, P., Kassaras, J., Diagourtas, D., Makropoulos, K., Veis, G., Papazisi, E., Mitsakaki, C., Karakostas, V., Papadimitriou, E., 1997. The Ms=6.2, June 15, 1995 Aigion earthquake (Greece): evidence for low-angle normal faulting in the Corinth rift. J. Seismol. 1, 131–150. https://doi.org/10.1023/A:1009795618839

Crampin, S., Booth, D.C., Evans, R., Peacock, S., Fletcher, J.B., 1990. Changes in shear wave splitting at Anza near the time of the North Palm Springs Earthquake. J. Geophys. Res. 95, 11197. https://doi.org/10.1029/JB095iB07p11197

Crampin, S., Zatsepin, S., 1997. Modelling the compliance of crustal rock—II. Response to temporal changes before earthquakes. Geophys. J. Int. 129, 495–506. https://doi.org/10.1111/j.1365-246X.1997.tb04489.x

Crampin, S., Volti, T., Stefánsson, R., 1999. A successfully stress-forecast earthquake. Geophys. J. Int. 138, F1–F5. https://doi.org/10.1046/j.1365-246x.1999.00891.x

Evangelidis, C.P., Triantafyllis, N., Samios, M., Boukouras, K., Kontakos, K., Ktenidou, O.-J., Fountoulakis, I., Kalogeras, I., Melis, N.S., Galanis, O., Papazachos, C.B., Hatzidimitriou, P., Scordilis, E., Sokos, E., Paraskevopoulos, P., Serpetsidaki, A., Kaviris, G., Kapetanidis, V., Papadimitriou, P., Voulgaris, N., Kassaras, I., et al., 2021. Seismic Waveform Data from Greece and Cyprus: Integration, Archival, and Open Access. Seismol. Res. Lett. https://doi.org/10.1785/0220200408

Gao, Y., Crampin, S., 2006. A stress-forecast earthquake (with hindsight), where migration of source earthquakes causes anomalies in shear-wave polarisations. Tectonophysics 426, 253–262. https://doi.org/10.1016/j.tecto.2006.07.013

Kapetanidis, V., Deschamps, A., Papadimitriou, P., Matrullo, E., Karakonstantis, A., Bozionelos, G., Kaviris, G., Serpetsidaki, A., Lyon-Caen, H., Voulgaris, N., Bernard, P., Sokos, E., Makropoulos, K., 2015. The 2013 earthquake swarm in Helike, Greece: seismic activity at the root of old normal faults. Geophys. J. Int. 202, 2044–2073. https://doi.org/10.1093/gji/ggv249

Kapetanidis, V., Kassaras, I., 2019. Contemporary crustal stress of the Greek region deduced from earthquake focal mechanisms. J. Geodyn. 123, 55–82. https://doi.org/10.1016/j.jog.2018.11.004

Kaviris, G., Spingos, I., Kapetanidis, V., Papadimitriou, P., Voulgaris, N., Makropoulos, K., 2017. Upper crust seismic anisotropy study and temporal variations of shear-wave splitting parameters in the Western Gulf of Corinth (Greece) during 2013. Phys. Earth Planet. Inter. 269, 148–164. https://doi.org/https://doi.org/10.1016/j.pepi.2017.06.006

References

Kaviris, G., Millas, C., Spingos, I., Kapetanidis, V., Fountoulakis, I., Papadimitriou, P., Voulgaris, N., Makropoulos, K., 2018. Observations of shear-wave splitting parameters in the Western Gulf of Corinth focusing on the 2014 Mw = 5.0 earthquake. Phys. Earth Planet. Inter. 282, 60–76. https://doi.org/10.1016/j.pepi.2018.07.005

Klein, F.W., 2002. User's guide to HYPOINVERSE-2000: a Fortran program to solve for earthquake locations and magnitudes. U.S. Geol. Surv. Prof. Pap., Open File Report rep. 02-17, 1–123.

Lambotte, S., Lyon-Caen, H., Bernard, P., Deschamps, A., Patau, G., Nercessian, A., Pacchiani, F., Bourouis, S., Drilleau, M., Adamova, P., 2014. Reassessment of the rifting process in the Western Corinth Rift from relocated seismicity. Geophys. J. Int. 197, 1822–1844. https://doi.org/10.1093/gji/ggu096

Rigo, A., Lyon-Caen, H., Armijo, R., Deschamps, A., Hatzfeld, D., Makropoulos, K., Papadimitriou, P., Kassaras, I., 1996. A microseismic study in the western part of the Gulf of Corinth (Greece): Implications for large-scale normal faulting mechanisms. Geophys. J. Int. 126, 663–688. https://doi.org/10.1111/j.1365-246X.1996.tb04697.x

Savage, M.K., Wessel, a., Teanby, N. a., Hurst, a. W., 2010. Automatic measurement of shear wave splitting and applications to time varying anisotropy at Mount Ruapehu volcano, New Zealand. J. Geophys. Res. Solid Earth 115. https://doi.org/10.1029/2010JB007722

Silver, P.G., Chan, W.W., 1991. Shear Wave Splitting and Sub continental Mantle Deformation. J. Geophys. Res. 96, 429–454. https://doi.org/10.1029/91JB00899

Sokos, E., Zahradník, J., Kiratzi, A., Janský, J., Gallovič, F., Novotny, O., Kostelecký, J., Serpetsidaki, A., Tselentis, G.A., 2012. The January 2010 Efpalio earthquake sequence in the western Corinth Gulf (Greece). Tectonophysics 530–531, 299–309. https://doi.org/10.1016/j.tecto.2012.01.005

Spingos, I., Kaviris, G., Millas, C., Papadimitriou, P., Voulgaris, N., 2020. Pytheas: An open-source software solution for local shear-wave splitting studies. Comput. Geosci. 134, 104346. https://doi.org/10.1016/j.cageo.2019.104346

Teanby, N., Kendall, J.-M., van der Baan, M., 2004. Automation of shear-wave splitting measurements using cluster analysis. Bulliten Seismol. Soc. Am. 94, 453–463. https://doi.org/10.1785/0120030123

Waldhauser, F., 2001. hypoDD-A Program to Compute Double-Difference Hypocenter Locations, U.S. Geol. Surv. Open File Rep. 01-113, 25 p.

Wüstefeld, A., Bokelmann, G., 2007. Null detection in shear-wave splitting measurements. Bull. Seismol. Soc. Am. 97, 1204–1211. https://doi.org/10.1785/0120060190